Endohedral metallofullerenes in self-assembled monolayers†

Maria del Carmen Gimenez-Lopez,[a] Jules A. Gardener,[b] Adam Q. Shaw,[b]
Agnieszka Iwasiewicz-Wabnig,[b] Kyriakos Porfyrakis,[b] Claire Balmer,[b]
Geraldine Dantelle,‡[b] Maria Hadjipanayi,[c] Alison Crossley,[b] Neil R. Champness,[a]
Martin R. Castell,[b] G. Andrew D. Briggs[b] and Andrei N. Khlobystov*[a]

A method has been developed for the attachment of a dithiolane group to endohedral metallofullerenes *via* a 1,3-dipolar cycloaddition reaction. This sulfur-containing functional group serves as an anchor, enabling efficient immobilisation of endohedral fullerenes on Au(111) surfaces at room temperature, directly from the solution phase. The functionalised fullerenes form disordered monolayers that exhibit no long-range ordering, which is attributed to both the strong bonding of the dithiolane anchor to the surface and to the conformational flexibility of the functional group. Endohedral fullerenes $Er_3N@C_{80}$ and $Sc_3N@C_{80}$ have been used as models for functionalisation and subsequent surface deposition. Their chemical reactivity towards dithiolane functionalisation and their surface behaviour have been compared to that of C_{60}. The endohedral fullerenes appear to be significantly less reactive towards the functionalisation than C_{60}, however they bind in a similar manner to a gold surface as their dithiolane terminated C_{60} counterparts. The optical activity of $Er_3N@C_{80}$ molecules is preserved after attachment of the functional group. We report a splitting of the endohedral Er^{3+} emission lines due to the reduction in symmetry of the functionalised fullerene cage, as compared to the highly symmetrical icosahedral C_{80} cage of pristine $Er_3N@C_{80}$.

Introduction

Carbon is a unique element that can create hollow, polyhedral cages called fullerenes. The void space within the fullerene cage can be occupied by a small heteroatom, such as N, P, He or a metal atom, or by a small metallic cluster.[1] Encapsulation of endohedral heteroatoms within fullerenes is a difficult task. These so-called "endohedral fullerenes" $X@C_N$ (where X is an atom or cluster incarcerated in the fullerene, and N is a number of carbon atoms in the fullerene cage) are usually formed in extremely low yields and require extensive purification, which hinders investigations of their properties and integration within functional materials.

The endohedral species in $X@C_N$ often possess useful magnetic or optical properties[1] that could potentially be utilised in nano-electronic devices.[2] In this case, the fullerene

cage serves as a "nanocontainer" which facilitates the incorporation of individual endohedral atoms within supramolecular architectures, such as 1D molecular chains in carbon nanotubes[2] or 2D molecular arrays on surfaces.[3] However, fullerene cages tend to have relatively isotropic exteriors owing to their spheroidal shapes, and so precise control of their positions and orientations can be difficult to achieve. An attractive approach for solving this problem is through chemical functionalisation of fullerene cages. This would allow for control over the orientation of the molecules *via* well-defined chemical bonding or highly directional non-covalent interactions. For example, endohedral fullerenes functionalised with an appropriate chemical group could be able to form spontaneous molecular monolayers on surfaces or molecular chains inside carbon nanotubes, within which the distance between the endohedral atoms X could be precisely controlled through the chemical functionality of fullerene cage.[4,5]

To demonstrate this principle, we have selected the most abundant type of endohedral fullerenes–trimetallic nitride templated endohedral metallofullerenes (TNT EMFs). These molecules comprise three endohedral metal atoms arranged in a triangular fashion around a nitrogen atom incarcerated in a C_{80} cage (Fig. 1). It is generally accepted that TNT EMFs $M_3N@C_{80}$ are stabilized by six electrons transferred from the trimetallic nitride (M_3N) cluster to the icosahedral (I_h) C_{80} carbon cage, resulting in a closed-shell electronic structure described as $[M_3N]^{6+}@[C_{80}]^{6-}$.[6-8] The transparency of the $[C_{80}]^{6-}$ cage for wavelengths longer that 1 μm, allows direct excitation of endohedral metal atoms, such as Er^{3+}, whose 4f
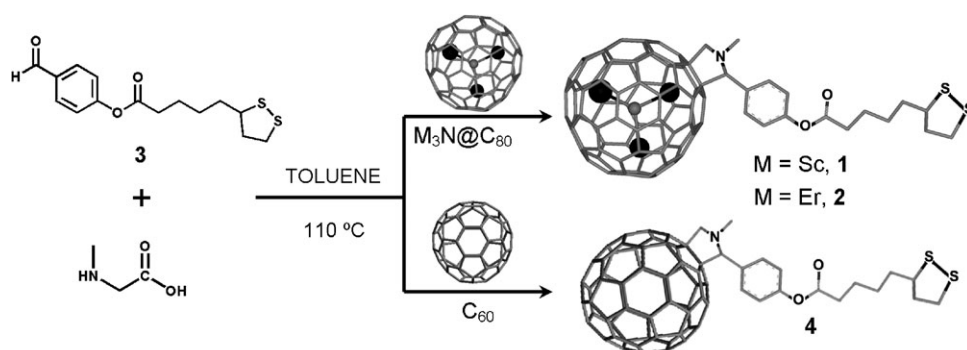
---

[a] *School of Chemistry, University of Nottingham, UK NG7 2RD.*
   E-mail: andrei.khlobystov@nottingham.ac.uk
[b] *Department of Materials, University of Oxford, Oxford,*
   UK OX1 3PH
[c] *Department of Physics, University of Oxford, Parks Road, Oxford,*
   UK OX1 3PU

Fig. 1 Cycloaddition of azomethine ylides to TNT EMFs and C_{60}. Endohedral metal atoms (black circles) are arranged in a triangular fashion around an endohedral nitrogen atom (grey circle).

electronic transitions occur in the near-IR range, important for telecommunications. Future technological applications of TNT EMFs may require the fabrication of well-ordered arrays of these fullerenes on surfaces. We demonstrate that a dithiolane group, which has a strong affinity for metal surfaces,[9] can be efficiently attached to $Sc_3N@C_{80}$ and $Er_3N@C_{80}$. We investigate the effects of the functional group on the optical properties of $Er_3N@C_{80}$ and the attachment of functionalised TNT EMFs to a gold surface.

Results and discussion

### Synthesis and characterization of dithiolane functionalized $M_3N@C_{80}$ (M = Sc, Er)

Synthesis and purification. We have explored the reactivity of TNT EMFs towards dithiolane functionalisation using the reaction of 1,3-dipolar cycloaddition of azomethine ylides (Fig. 1). The cycloaddition reactions are commonly used for functionalisation of fullerene cages, as they often yield isomerically pure products with high efficiency. However, one of the main drawbacks of cycloaddition reactions is the problem of addition of multiple functional groups to a fullerene cage.

In order to address this problem, the reaction progress was carefully monitored by thin layer chromatography (TLC) and matrix-assisted laser desorption/ionization time-of-flight mass spectrometry (MALDI-TOF MS, see Supporting Information file). Fullerene C_{60} appears to react smoothly with the dithiolane aldehyde **3** at 110 °C, forming a fullerene functionalised with one dithiolane group $C_{60}R$ (where R is a functional group), and subsequent products of bis-$C_{60}(R)_2$, tris-$C_{60}(R)_3$ and tetra-functionalised $C_{60}(R)_4$ fullerene (Fig. 2a). The reactivities of C_{70} and a higher fullerene C_{78} (Supporting Information file) appear to be significantly lower than C_{60} (Fig. 2b), which can be attributed to the fact that the proportion of reactive carbon–carbon bonds within the fullerene structure becomes lower as the fullerene cage becomes larger.[10]

Since the cycloaddition takes place on the timescale of hours, the number of dithiolane groups appended to the fullerene cage can be conveniently controlled by the duration of the reaction. If the rate of formation of the mono-functionalised product is known, the yield of this product can be optimised by quenching the reaction before the bis-functionalised fullerene is formed in significant quantities. We adopted this strategy for

the synthesis of pyrrolidinofullerene derivate N-methyl-2-(4-(liponyloxy)benzyl)-$Sc_3N@C_{80}$ (**1**), which was formed from $Sc_3N@C_{80}$, dithiolane aldehyde **3** and sarcosine at 110 °C (Fig. 1). The reactivity of the endohedral fullerene $Sc_3N@C_{80}$ towards 1,3-dipolar cycloaddition appears to be significantly lower than that of C_{60}, and is comparable to that of higher fullerenes of similar size. However, $Sc_3N@C_{80}$ does not entirely support the trend (Fig. 2b), showing a slightly higher reactivity than a smaller fullerene C_{78}, which may be related to the presence of the endohedral group Sc_3N inside C_{80}. The effects of Sc_3N on the reactivity of the fullerene cage are difficult to evaluate directly, as the empty C_{80}-I_h fullerene does not exist. Mono-adduct **1** was isolated with a 34% yield after purification by column chromatography. Negative mode MALDI-TOF mass spectrum of pure **1** (Fig. 3b) shows a pronounced M$^-$ peak at 1447.14 m/z and only a small degree of fragmentation leading to $Sc_3N@C_{80}$ at 1109.72 m/z.

TNT EMFs with the same structure of the fullerene cage are expected to have similar chemical reactivity. We have therefore used the optimised conditions found for the dithiolane addition reaction with $Sc_3N@C_{80}$ for functionalisation of $Er_3N@C_{80}$ without further modification. Mono-functionalised $Er_3N@C_{80}$**2** was isolated in a 28% yield following the same procedure as for fullerene **1**. The product **2** was observed clearly in MALDI-TOF mass spectrum (negative ionisation mode) as a M$^-$ peak at 1815.53 m/z (Fig. 4a). It is interesting that the fullerene **2** undergoes a more extensive fragmentation in the mass spectrometer, using the same conditions, than fullerene **1**; the peaks at 1682.51, 1658.45 and 1522.79 m/z emerge as a result the breakage of dithiolane functional group. The molecular peak of the mono-functionalised **2** is approximately twice as broad as that of **1**. This is due to the wider isotopic distribution of erbium as compared to scandium, which is in a good agreement with the calculated distributions. High performance liquid chromatography (HPLC) through a 5PYE column (Nacalai Tesque) with toluene as eluent (flow rate 7 ml min^{-1}) showed a retention time of 3.25 min for **2** (Fig. 4b) that is significantly shorter than the retention time observed for pristine $Er_3N@C_{80}$ under the same conditions (10.93 min, Fig. 4c). The dithiolane containing functional group attached to the carbon cage is quite polar and somewhat hydrophilic. This is expected to reduce the retention time in a reversed phase HPLC column. Moreover, the symmetry of the C_{80} cage is broken by the functional group, which could induce a
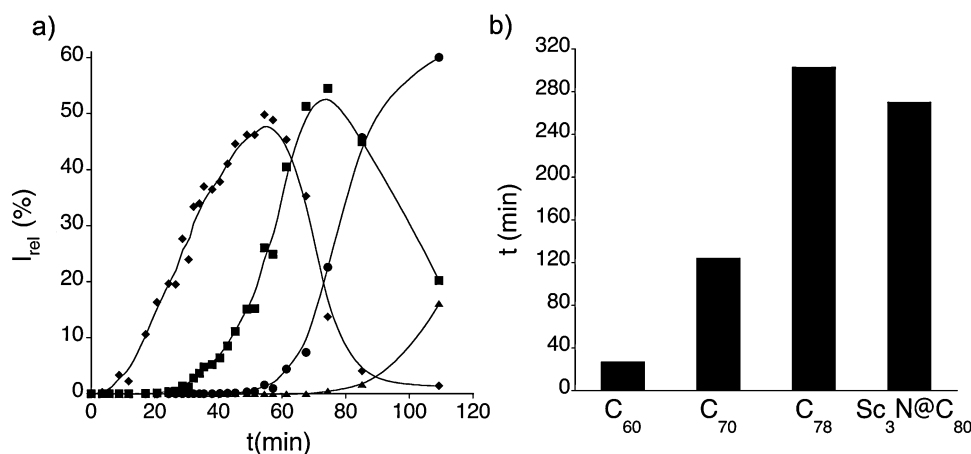
Fig. 2 (a) Evolution of mono- (♦), bis- (■), tris- (●) and tetra-functionalised (▲) fullerenes in the reaction of 1,3-dipolar cycloaddition of dithiolane aldehyde **3** with C_{60} as a function of time. I_{rel} is a relative conversion rate calculated as I_{rel} (%) = $[I_{adduct}/(\sum I_{adduct(i)} + I_{C60})] \times 100$ measured by MALDI-TOF mass spectrometry. (b) Time required for bis-functionalised fullerene $C_N(R)_2$ to emerge in the reaction of 1,3-dipolar cycloaddition measured for different fullerenes.
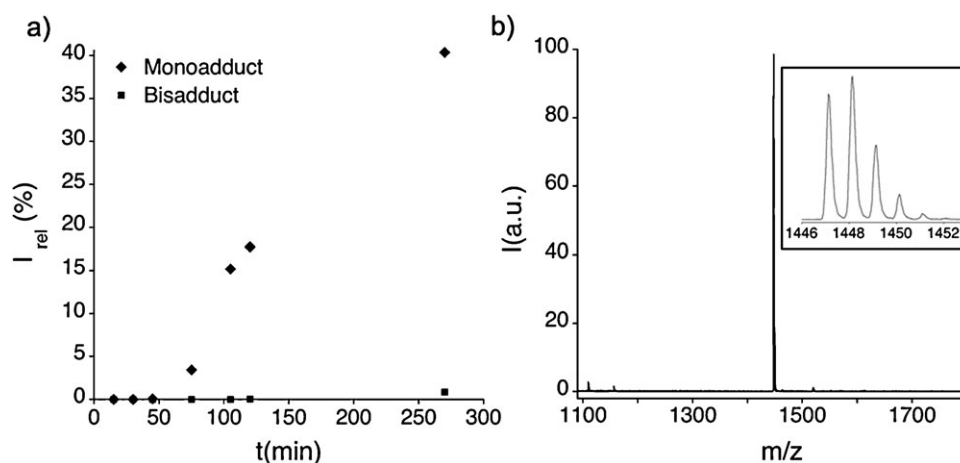

Fig. 3 (a) Evolution of the mono- and bis-functionalised $Sc_3N@C_{80}$ at 110 °C as a function of the reaction time. (b) MALDI-TOF mass spectrum of purified **1** (inset: isotopic distribution pattern confirming the composition of monoadduct **1**).

substantial dipole moment on the cage. The purity of the product **2** was estimated to be at least 98% by HPLC. The absence of secondary peaks after 5 cycles of HPLC in a recycling mode confirm that **2** is formed as a single isomer.

NMR. The five-member pyrrolidine ring is directly attached to the carbon cage (Fig. 5), rendering analysis of ^{1}H and ^{13}C NMR spectra of the pyrrolidine group very important for understanding the molecular structures of the functionalised metallofullerenes.[11–18] The ^{1}H NMR spectrum of **1** indicates the presence of a single regioisomer. The signals for the pyrrolidine ring geminal protons H^a and H^b in **1** are separated by 1.3 ppm and appear as two doublets at δ = 4.38 and 3.08 ppm (J = 9.7 Hz). The remaining pyrrolidine ring proton H^c gives a singlet peak at δ = 3.76 ppm, while for the N-methyl group H^d atoms a singlet is observed at δ = 3.15 ppm. The heteronuclear multiple quantum correlation (HMQC) spectrum (ESI)† enables correlation of the chemical shifts of the carbon atoms with corresponding hydrogen atoms attached to them, as summarised in Table 1. The relatively large difference in the chemical shifts of the geminal hydrogen atoms H^a and H^b,

coupled with the presence of only one set of pyrrolidine carbon atoms, suggest the formation of a product where the pyrrolidine ring is attached to a [5,6]-bond of the C_{80} cage, (Fig. 5), similar to other examples of 1,3-dipolar cycloaddition reported for TNT EMFs.[11–18] In the case of C_{60}, where the cycloaddition reactions are known to take place at a [6,6]-bond, the mono-functionalised N-methyl-2-(4-(liponyloxy)benzyl)-[6,6]-C_{60} (**4**) has a much smaller difference between the chemical shifts of the geminal hydrogen atoms H^a and H^b of the pyrrolidine ring ($\Delta\delta$ = 0.7 ppm). This is because the H^a and H^b of the [6,6]-adduct **4** occupy more similar positions to those of the [5,6]-adduct **1** (Fig. 5).

Raman spectroscopy. The Raman spectrum of **2** under a 532 nm laser excitation (Fig. 6) shows several peaks in the range of 450–750 cm^{-1}, typical for the CS-SC moiety (Table 2). The frequencies of these modes are known to vary substantially depending on the precise structure of a 'CS–SC'-containing compound,[19] making a complete peak assignment difficult in this case. Nevertheless, a well-defined peak observed at 498 cm^{-1} is within the known range of the S–S bond
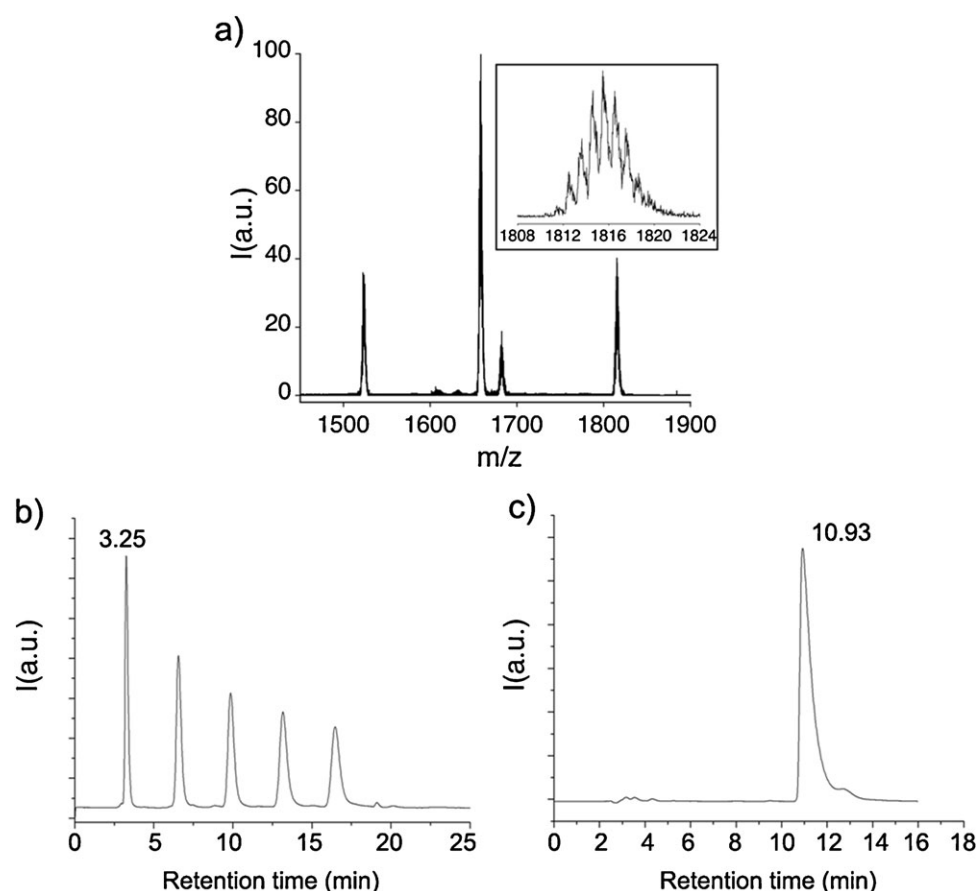
Fig. 4 MALDI-TOF mass spectrum (a) and recycling-HPLC trace (b) of the purified product **2**. The retention time of **2** is 3.25 min. After 5 cycles no other peaks were detected. The retention time of **2** is significantly shorter than that of pristine $Er_3N@C_{80}$, under the same conditions (c).
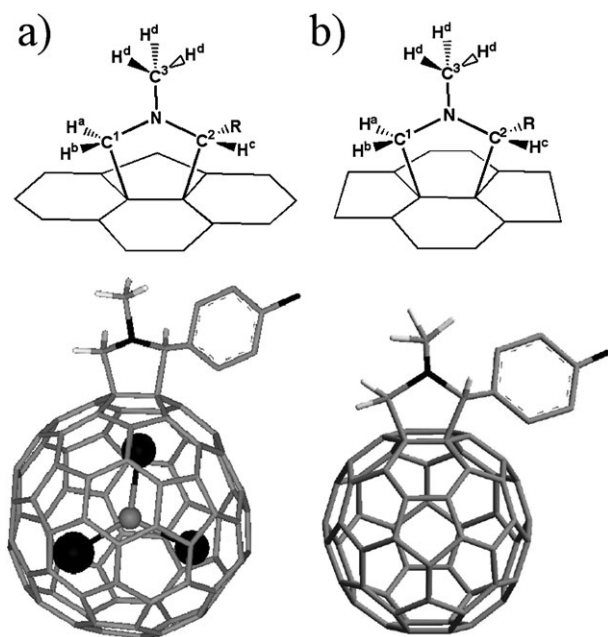
Fig. 5 Structural diagrams of pyrrolidine ring attached to [5,6]-bond of $Sc_3N@C_{80}$ (a) and [6,6]-bond of C_{60} (b).

vibration at 470–530 cm^{-1}. The Raman peaks at 653 cm^{-1} and 659 cm^{-1} (Fig. 6) can be attributed to the C–S bonds of **2**.

A further proof of successful $Er_3N@C_{80}$ functionalisation is provided by Raman peaks at ~3000 cm^{-1} (see inset in Fig. 6), indicating the presence of C–H bonds associated with the pyrrolidine, the dithiolane groups and the linking alkyl chain ($-CH_2-)_4$.

Photoluminescence of dithiolane functionalized $Er_3N@C_{80}$ (2) in solution

In order to gain an insight into the influence of the functional group on the inherent properties of the incarcerated species, comparative photoluminescence measurements of $Er_3N@C_{80}$ or **2** in solution have been performed. Optical excitation of the fullerene cage leads to population in the $Er^{3+}\,^4I_{13/2}$ state via a series of incoherent non-radiative relaxation processes.[20] Subsequent radiative relaxation occurs to the $^4I_{15/2}$ manifold. The emitted photons are of wavelengths beyond the window in which the fullerene cage is absorbing, thus permitting their detection. The photoluminescence spectra of $Er_3N@C_{80}$ and **2** (Fig. 7) comprise a series of sharp lines corresponding to the emission from the lowest sublevel of $^4I_{13/2}$, the only sublevel populated at 5 K, down to the different sublevels of the $^4I_{15/2}$ ground state. Those sublevels arising from the crystal field splitting of the $^4I_{13/2}$ and $^4I_{15/2}$ Er^{3+} states are relatively sensitive to the Er^{3+} local environment in comparison to other sublevels.[21] The emission lines of $Er_3N@C_{80}$ are monocomponent in nature (Fig. 7), whereas those of **2** are further

Table 1 Chemical shifts of H and C atoms of pyrrolidine rings in $Sc_3N@C_{80}$ (**1**) and C_{60} (**4**)

Part of pyrrolidine ring	Chemical shifts in **1**/ppm	Chemical shifts in **4**/ppm
CH_2 group	H^a 4.4, H^b 3.1, C^1 72.5	H^a 5.0, H^b 4.3, C^1 70.1
CH group	H^c 3.8, C^2 85.0	H^c 4.9, C^2 83.0
CH_3 group	H^d 3.1, C^3 41.4	H^d 2.8, C^3 40.0
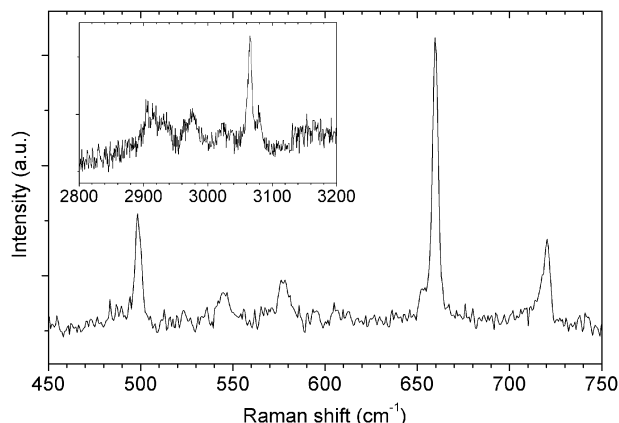
Fig. 6 Raman spectrum of **2** under 532 nm laser excitation, confirming the functionalisation. Raman shifts in the ranges typical for CS–SC (main plot), and C–H (inset) bond associated vibrations are shown.

Table 2 Comparison of Raman peak positions in the range of 450–750 cm^{-1} for **2** and compounds containing similar CS–SC groups[19] (peaks associated with S–S bond are highlighted in bold)

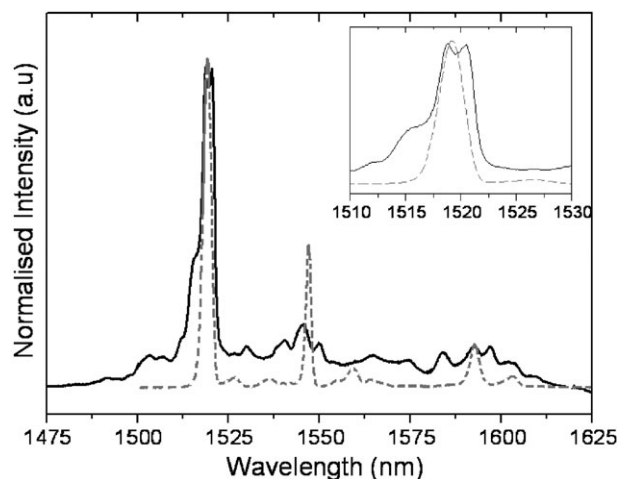| **2**/cm^{-1}	D,L-6,8-thioctic acid amide/cm^{-1}	D,L-6,8-thioctic acid/cm^{-1}
498	**496**	456
546	504	$\sim$**501**
578	533	511
653	585	559
659	664	634
720	675	682
	708	

Fig. 7 Photoluminescence spectra of **2** (solid) and $Er_3N@C_{80}$ (dashed) in CS_2 solutions at 5 K under 532 nm excitation. The inset shows the most intense emission line at $\sim$1520 nm in greater detail, highlighting the splitting of **2**.

split. In $Er_3N@C_{80}$, all Er^{3+} of the Er_3 cluster occupy equivalent positions inside the C_{80} cage.[22] In the case of **2**, the functional group reduces the C_{80} cage symmetry and therefore perturbs the local environment of each Er^{3+} inside the cage. Although the presence of the functional group does not quench the luminescence of endohedral atoms, it appears to make the endohedral metal atoms in the trigonal Er_3N cluster non-equivalent, which is manifested in the observed splitting of their emission peaks.

Deposition of ditholane functionalised $Er_3N@C_{80}$ (2) onto a gold surface

Deposition method. To evaluate the affinity of the functionalised TNT EMFs to metal surfaces and their ability to form thin films, we have studied the deposition of **2** and **4** on a gold surface by immersing freshly prepared Au/mica substrates in dilute solutions of fullerenes.

Surface topography. We have assessed the topography of the dithiolane functionalised $Er_3N@C_{80}$**2** self-assembled monolayers on Au(111) using scanning tunnelling microscopy (STM) (Fig. 8(a) and (b)). Spherical features are observed

across the sample surface. The apparent diameters of these features range from 1.1 nm to 2.6 nm. Typically, the diameters of unfunctionalised TNT EMFs in close packed arrays are $\sim$1.15 nm.[23,24] However, in our case the molecules are not densely packed and so tip convolution is likely to broaden their appearance. In addition, the functional group is conformationally flexible and so the fullerene cages are likely to move due to interactions between the STM tip and the fullerenes. This movement will significantly affect the measured fullerene diameter and increase the range of measured values. Our observations are consistent with these expectations, and therefore we attribute each spherical feature in Fig. 8(a) and (b) as a carbon cage of functionalised $Er_3N@C_{80}$.

Large areas of the surface are reasonably uniformly covered with a monolayer or sub-monolayer of **2** (Fig. 8). Unfunctionalised TNT EMFs deposited on Au-substrates from the solution phase under similar conditions show much less uniform coverage of the substrate, typically aggregating and forming multilayered islands on Au(111). As expected, the dithiolane group attached to the fullerene cage increases the affinity of fullerene to the metal surface and facilitates the formation of a fullerene monolayer. However, no long-range ordering of the molecules has been observed for monolayers of functionalised fullerenes. We attribute this observation to the strong bonding between the dithiolane group and the Au(111) surface. It is likely that two S–Au bonds per each molecule of **2** largely immobilise the functionalised fullerenes and so they remain at or close to their initial adsorption sites, preventing the surface migration of the molecules and formation of an ordered array. However, isolated patches comprising close
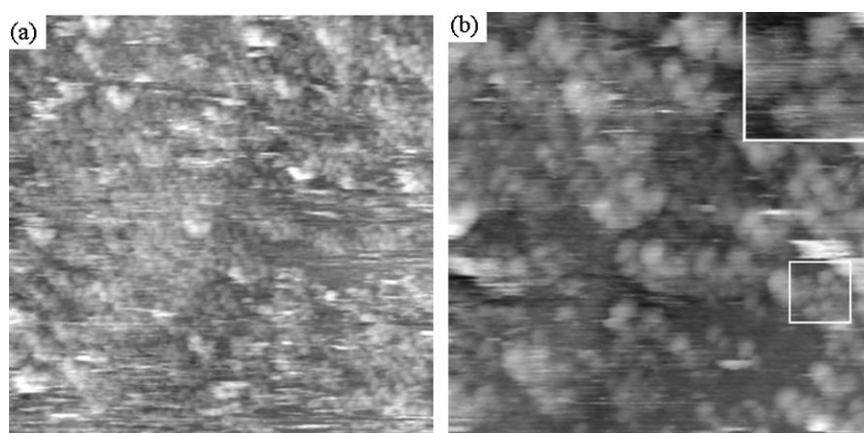
Fig. 8 Scanning tunnelling microscopy images of dithiolane functionalised Er₃N@C₈₀**2** on Au(111). Spherical features are observed and these are attributed to the fullerene cages of the molecules. (a) A large scan area image (70 × 70 nm) showing that the layer is almost complete. (b) A more detailed image (40 × 40 nm) in which the positions of individual molecules can be identified. A small close-packed cluster is highlighted by a white square and is shown in the inset.

packed fullerenes are occasionally seen illustrating the possibility of short-range molecular ordering (Fig. 8b, inset).

Bonding to the surface. To explore further the mechanisms of the surface bonding for functionalised fullerenes, we have taken advantage of the high surface sensitivity and detailed chemical information that are offered by X-ray photoelectron spectroscopy (XPS). In general, sulfur-terminated functionalised fullerenes can bind to an Au(111) surface *via* either the functionalised group or the fullerene cage, leading to a range of possible geometries.[25] XPS can be used to determine the orientation of the dithiolane functionalised fullerene monolayers with respect to the Au(111) surface. In particular, the S2p peaks provide excellent indicators of whether or not the functional group is bound to Au.

High resolution XPS spectra of functionalised fullerenes **2** and **4** show a good agreement in lineshape of the core level S2p peaks (Fig. 9), suggesting that the S atoms of dithiolane group have similar chemical environment in both cases (the tail towards higher energies for fullerene **2** is due to the onset of the Er 4d peak). Spectral fitting shows the presence of $S2p_{3/2}$ ($S2p_{1/2}$) peaks at 161.9 eV (163.1 eV) and 161.7 eV (162.9 eV) for the dithiolane functionalised Er₃N@C₈₀ and C₆₀ monolayers, respectively. These values are in good agreement with the known spectral lines for S-atoms covalently bound to Au,[25] and unequivocally demonstrate that the dithiolane group forms two S–Au bonds with the surface (Fig. 10). This binding mode provides a very efficient interaction of functionalised fullerenes with the surface, that is expected to be twice as strong as the standard Au–thiol interaction typically utilised for self-assembled monolayers. This confirms that the lack of long-range order in the monolayers of **2** and **4** is related to the strong interaction of the dithiolane group with the metal surface.

Surface photoluminescence of dithiolane functionalized Er₃N@C₈₀ (2) on Au(111)

The photoluminescence spectrum of dithiolane functionalised Er₃N@C₈₀ deposited on Au(111) surface was compared to
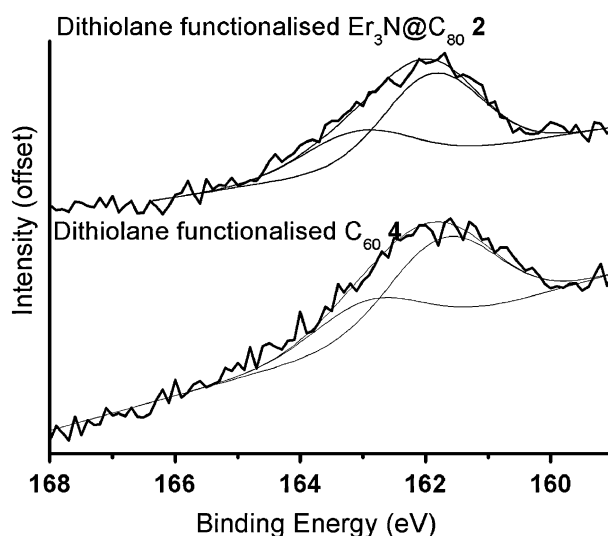
Fig. 9 S2p core level peak in XPS spectra of self-assembled monolayers of dithiolane functionalised Er₃N@C₈₀ (**2**) and dithiolane functionalised C₆₀ (**4**) on Au(111). The peak intensity is offset for clarity. Gaussian peak fits are included.
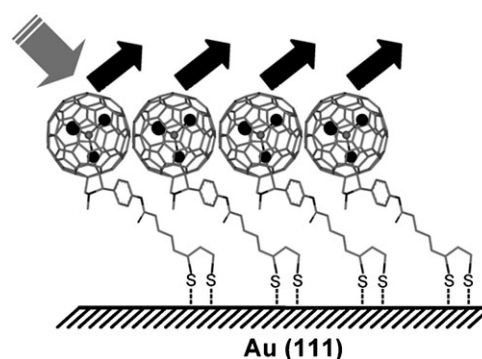
Fig. 10 Schematic representation of bonding of the dithiolane group to the Au-surface.

that in solution (Fig. 11). An excellent agreement between the peak positions is observed, verifying that the optical
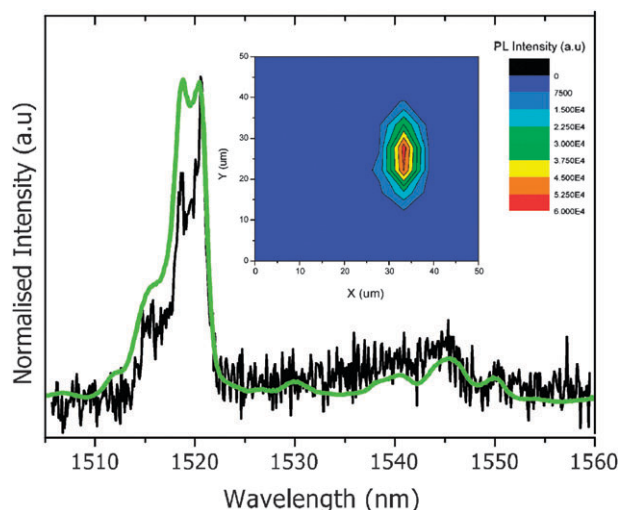
Fig. 11 Photoluminescence of **2** deposited on a Au(111) surface under a 800 nm laser excitation (black). The spectrum of **2** in CS_2 as shown in Fig. 7 is included for comparison (green). A typical fluorescence map (50 × 50 μm) of **2** on Au(111) is shown in the inset.

functionality and chemical integrity of this fullerene have been retained. Variations in the relative intensities of the peaks are observed (this is particularly apparent for the ~1519 nm emission line). These differences could arise from the preferential molecular orientation with respect to the substrate imposed by the Au–S bonds. We note that spatial mapping has highlighted inhomogeneities in the surface coverage, with photoluminescence signal only obtained from isolated regions of approximately 10 μm in diameter (an example of which is shown in the inset of Fig. 11). These patches are likely to arise from the regions of higher surface concentration of **2**, possibly attracted to defect sites of the Au film.

Conclusions

Endohedral metallofullerenes have been functionalised with sulfur-containing groups for the first time and their inter-actions with gold surfaces have been explored. We have developed a method of attachment of dithiolane groups to $Er_3N@C_{80}$ and $Sc_3N@C_{80}$ TNT fullerenes, and have isolated isomerically pure, mono-functionalised endohedral fullerenes. The presence of the sulfur-containing group on TNT fullerenes has a significant effect on the interactions of these fullerenes with gold surfaces. The functionalised fullerenes deposited from solution give a more complete coverage of Au(111) surfaces than unfunctionalised TNT fullerenes, due to strong bonding between the dithiolane group and the metal surface. The effects of the exohedral functional group on the photoluminescence properties of the endohedral atoms have been demonstrated for the first time using $Er_3N@C_{80}$ as a model. The addition of chemical functionality to the highly symmetrical icosahedral C_{80} cage lowers the symmetry of the fullerene and results in splitting the major PL peaks of the endohedral Er-atoms. This may give a potential mechanism for controlling the functional properties of EMFs *via* the exohedral chemical functionality. The exohedral functionality does not quench the luminescence of the EMFs, so that the

functionalised $Er_3N@C_{80}$ retains its optical properties within a monolayer assembled on the surface. The methodology for chemical functionalisation and surface deposition of EMFs described in this study can be further extended to electron spin active fullerenes, and in the long term could enable incorporation of endohedral fullerenes in functional electronic devices, harnessing their unique physicochemical properties for future technological applications.

Experimental

Sample preparation

Raw erbium and scandium TNTs were supplied by Luna Innovations. Erbium TNTs were further purified by high performance liquid chromatography (HPLC) using a 5PYE column (Nacalai Tesque). Only one isomer of $Er_3N@C_{80}$ was detected. All other reagents and solvents were purchased from Aldrich and were used without further purification. All reactions were carried out under an argon atmosphere. Elemental analyses (C, H, N) were performed by the Elemental Analysis Service of London Metropolitan University. Infrared spectra were measured as either KBr discs or in solution on a Nicolet Avatar 380 FT-IR spectrometer over the range 400–4000 cm^{-1}. ^{1}H and ^{13}C NMR spectra were obtained on a Bruker DPX300, 400, and AV(III)500 spectrometers. Coupling constants (J) are denoted in Hz, and chemical shifts (δ), in ppm. Multiplicities are denoted as follows: s = singlet, d = doublet, m = multiplet. Mass spectrometry was carried out on a Bruker Ultraflex III MALDI-TOF spectrometer using DCTB as matrix (355 nm) and on a Bruker MicroTOF with electrospray ionization (ESI). Analytical thin-layer chromatography (TLC) was performed using aluminium-coated Merck Kieselgel 60 F254 plates.

Dithiolane aldehyde precursor. 4-(Liponyloxy)benzaldehyde **3** was synthesized according with the procedure shown in the Supporting Information.

N-Methyl-2-(4-(liponyloxy)benzyl)-Sc₃N@C₈₀ fulleropyrrolidine (1). 0.8 mg of $Sc_3N@C_{80}$ (7.6 × 10^{-4} mmol), 1.1 mg of sarcosine (0.013 mmol) and 13.0 mg of 4-(liponyloxy)-benzaldehyde (0.04 mmol) were dissolved in 15 mL of dry toluene in a 50 mL two-neck Schlenk flask equipped with a magnetic stirrer under argon. The mixture was heated and stirred for 270 min at 110 °C using an oil bath. After cooling to room temperature, the solvent was evaporated under reduced pressure until the volume was approximately 10 mL The reaction mixture was purified using silica gel column and toluene as eluent (R_f 0.13). After evaporation, 0.45 mg of a black powder was obtained (34% yield). MALDI-MS 1447.14 m/z [M]$^-$.

N-methyl-2-(4-(liponyloxy)benzyl)-Er₃N@C₈₀ fulleropyrrolidine (2). Following the procedure for the synthesis of **1**, 1.8 mg of $Er_3N@C_{80}$ (1.2 × 10^{-3} mmol), 1.6 mg of sarcosine (0.018 mmol) and 18.5 mg of 4-(liponyloxy)benzaldehyde (0.06 mmol) were refluxed. The crude mixture was purified by column chromatography (silica, toluene) (R_f 0.14) to give **2** (0.55 mg) as a dark solid in 28% yield. MALDI-MS

1815.53 m/z [M]$^-$. HPLC (5PYE column, 10 mm × 250 mm, 7 mL min^{-1} toluene, $\lambda = 312$ nm): 3.25 min.

N-methyl-2-(4-(liponyloxy)benzyl)-[6,6]-C$_{60}$ fulleropyrrolidine (4). A solution of 4-(liponyloxy)benzaldehyde (51.6 mg, 0.16 mmol) dissolved in dry toluene (5 mL) was added dropwise with stirring to a solution of C$_{60}$ (100 mg, 0.14 mmol) and sarcosine (61.8 mg, 0.7 mmol) in dry toluene (35 mL). The resultant solution was refluxed at 110 °C under argon for 14 h. After cooling to room temperature, the solvent was evaporated, and the crude mixture was purified by column chromatography (silica, toluene) (R_f 0.22). Further purification was accomplished by subsequent precipitation with methanol to give **3** as a brown solid in 37% yield. ^{1}H NMR {400 MHz, CDCl$_3$, 300 K} δ_H 7.17 (m, 4H, aromatic H), 5.03 (d, $J = 9.3$ Hz, 1H, –CH$_2$ pyrrolidine), 4.99 (s, 1H, –CH pyrrolidine), 4.33 (d, $J = 9.3$ Hz, 1H, –CH$_2$ pyrrolidine), 3.57 (m, 1H, –CH), 3.20–3.10 (m, 2H, –CH$_2$), 2.59 (t, $J = 7.0$ Hz, 2H, –CH$_2$– alkyl chain), 2.49 (m, 1H, –CH$_2$), 1.96 (m, 1H, –CH$_2$), 1.76 (m, 2H, –CH$_2$– alkyl chain), 1.61 (m, 2H, –CH$_2$– alkyl chain) ppm. ^{13}C NMR {500 MHz, CDCl$_3$, 300 K} δ_C 170.70, 150.21, 148.41, 147.37, 146.63, 146.45, 146.37, 146.30, 146.22, 146.10, 146.0, 145.81, 145.34, 144.70, 144.47, 143.23, 142.72, 142.24, 142.32, 142.14, 82.91, 70.10, 68.95, 68.41, 40.04, 34.02, 33.40, 28.15, 26.60, 24.75 ppm. MALDI-MS 1057.61 m/z [M]$^-$. Elemental analysis found (expected)%: C 87.32 (87.32), H 2.16 (2.28), N 1.28 (1.32). IR (KBr disk) 2922 m (–C–H alkyl chain), 1740 m (–COO–), 1458 m (C=C (s) phenyl group), 1384 (–O–CO–CH$_2$–), 1458 m (C=C (b) phenyl group). UV–vis (CHCl$_3$) λ_{max}: 431.66, 700. HPLC (SiO$_2$ FORTIS HILIC (5μ) column, 250 mm × 21 mm, 5 mL min^{-1} 3% ethylacetate in toluene, $\lambda = 254$ nm): 3.15 min (ESI).‡

Raman spectroscopy

Functionalised fullerenes were dissolved in CS$_2$. The solution was drop coated on to a glass optical slide and dried in air. The Raman spectra were collected using a Horiba Jobin-Yvon Lab Aramis Confocal Raman Microscope in backscattering geometry, with an x100SLW objective (300 μm working distance). Measurements were performed at room temperature, under 532 nm excitation (solid state laser), on relatively thick (multi-layered film) sample areas.

Photoluminescence measurements

PL in solution. Functionalised fullerenes were dissolved in CS$_2$. The solution was placed in a quartz tube, degassed and sealed. For comparison, an Er$_3$N@C$_{80}$ solution was prepared in a similar manner. The concentration of each solution was not determined but was kept relatively low to avoid any clustering. Photoluminescence measurements were performed under a 532 nm excitation (15 mW), at 5 K using a He Oxford Instruments CF204 continuous flow cryostat. The detection was done through a monochromator (600 lines/nm grating) equipped with an InGaAs array detector.

PL on surface. Samples comprising Er$_3$N@C$_{80}$**2** on Au(111) were prepared as outlined in the section "deposition of functionalised fullerenes on Au-substrates" below. PL measurements on these thin film samples were performed

using a confocal microscope with an ×100 objective (Mitutoyo, 0.5 NA), which was mounted on a piezoelectric XYZ-stage 1 nm resolution. The samples were placed inside a continuous-flow liquid He microscope cryostat (Janis ST-500) in order to do the measurements at 5 K. The excitation was performed using a 800 nm Ti:Sapphire laser (Spectra-physics Mai-Tai). The detection was carried out through a monochromator (1200 lines/nm grating) equipped with the same InGaAs detector.

Surface deposition and characterisation

Deposition of functionalised fullerenes on Au-subsrtates. Au(111) films (thickness 150 nm) grown on mica were used for the surface studies. These were prepared by flame annealing the substrate, a procedure well-known to produce the characteristic herringbone reconstruction of this surface. Thin film samples were prepared by immersing freshly prepared Au/mica substrates in dilute solutions of dithiolane functionalised C$_{60}$**4** and Er$_3$N@C$_{80}$**2** in toluene and drying in a nitrogen gas stream.

STM. STM images were obtained from an ultra high vacuum (UHV) JEOL JSTM4500S scanning tunnelling microscope (base pressure ∼10^{-9} mbar). The samples were prepared using the aforementioned *ex situ* procedure, immediately before transferring to the UHV chamber. Images were taken at room temperature at +2.3 V (bias applied to sample) and 0.2 nA using electrochemically etched tungsten tips.

XPS. X-ray photoelectron spectroscopy measurements were performed using a VG Michrotech CLAM 4 MCD analyser system with a pass energy of 20 eV and slit size of 5 mm. X-rays were provided from a Mg Kα X-ray source operated at 200 W (base pressure ∼10^{-10} mbar), whilst data was obtained using SPECTRA version 8 operating system. A Shirley background subtraction was applied to all peaks prior to fitting. Binding energy scales were referenced using standard values for the Au4f$_{7/2}$ (84.0 eV), Au4f$_{5/2}$ (87.7 eV) and C1s (284.5 eV) peaks of gold and fullerenes, respectively. S2p$_{1/2}$ and S2p$_{3/2}$ peak fitting was performed whilst constraining the binding energy separation and relative peak abundances to values expected from spin–orbit coupling (1.2 eV and 1 : 2, respectively).

Acknowledgements

References

1 H. Shinohara, *Rep. Prog. Phys.*, 2000, **63**, 843–892.
2 A. N. Khlobystov, D. A. Britz and G. A. D. Briggs, *Acc. Chem. Res.*, 2005, **38**, 901–909.
3 J. A. Theobald, N. S. Oxtoby, M. A. Phillips, N. R. Champness and P. H. Beton, *Nature*, 2003, **424**, 1029–1031.
4 T. W. Chamberlain, A. Camenisch, N. R. Champness, G. A. D. Briggs, S. C. Benjamin, A. Ardavan and A. N. Khlobystov, *J. Am. Chem. Soc.*, 2007, **129**, 8609–8614.

5 T. W. Chamberlain, R. Pfeiffer, H. Peterlik, H. Kuzmany, F. Zerbetto, M. Melle-Franco, L. Staddon, N. R. Champness, G. A. D. Briggs and A. N. Khlobystov, *Small*, 2008, **4**, 2262–2270.

6 M. M. Olmstead, A. de Bettencourt-Dias, J. C. Duchamp, S. Stevenson, D. Marciu, H. C. Dorn and A. L. Balch, *Angew. Chem., Int. Ed.*, 2001, **40**, 1223–1225.

7 K. Kobayashi, Y. Sano and S. Nagase, *J. Comput. Chem.*, 2001, **22**, 1353–1358.

8 L. Alvarez, T. Pichler, P. Georgi, T. Schwieger, H. Peisert, L. Dunsch, Z. Hu, M. Knupfer, J. Fink, P. Bressler, M. Mast and M. S. Golden, *Phys. Rev. B: Condense. Matter Mater. Phys.*, 2002, **66** 035107/1–035107/7.

9 T. Weider, F. Bretthauer, N. Ballav, H. Motschmann, H. Orendi, C. Brufn, U. Siemeling and M. Zharnikov, *Langmuir*, 2008, **24**, 11691–11700.

10 T. Oshima, H. Kitamura, T. Higashi, K. Kokubo and N. Seike, *J. Org. Chem.*, 2006, **71**, 2995–3000.

11 E. B. Iezzi, K. H. Duchamp, T. E. Glass, H. M. Lee, M. M. Olmstead, A. L. Balch and H. C. Dorn, *J. Am. Chem. Soc.*, 2002, **124**, 524–525.

12 H. M. Lee, M. M. Olmstead, E. Iezzi, J. C. Duchamp, H. C. Dorn and A. L. Balch, *J. Am. Chem. Soc.*, 2002, **124**, 3494–3495.

13 C. M. Cardona, A. Kitaygorodskiy, A. Ortiz, M. A. Herranz and L. Echegoyen, *J. Org. Chem.*, 2005, **70**, 5092–5097.

14 C. M. Cardona, A. Kitaygorodskiy and L. Echegoyen, *J. Am. Chem. Soc.*, 2005, **127**, 10448–10453.

15 T. Cai, Z. Ge, E. B. Iezzi, T. E. Glass, K. Harich, H. W. Gibson and H. C. Dorn, *Chem. Commun.*, 2005, 3594–3596.

16 T. Cai, C. Slebodnick, L. Xu, K. Harich, T. E. Glass, C. Chancellor, J. C. Fettinger, M. M. Olmstead, A. L. Balch, H. W. Gibson and H. C. Dorn, *J. Am. Chem. Soc.*, 2006, **128**, 6486–6492.

17 C. M. Cardona, E. Bevan and L. Echegoyen, *J. Am. Chem. Soc.*, 2006, **128**, 6480–6485.

18 J. R. Pinzon, M. E. Plonska-Brzezinska, C. M. Cardona, A. J. Athans, S. Shankara Gayathri, D. M. Guldi, M. A. Herranz, N. Martin, T. Torres and L. Echegoyen, *Angew. Chem., Int. Ed.*, 2008, **47**, 4173–6.

19 H. E. Van Wart, A. Lewis, H. A. Scheraga and F. D. Saevat, *Proc. Natl. Acad. Sci. U. S. A.*, 1973, **70**, 2619.

20 M. A. G. Jones, R. A. Taylor, A. Ardavan, K. Porfyrakis and G. A. D. Briggs, *Chem. Phys. Lett.*, 2006, **428**, 303–306.

21 A. Tiwari, G. Dantelle, K. Porfyrakis, R. A. Taylor, A. A. R. Watt, A. Ardavan and G. A. D. Briggs, *J. Chem. Phys.*, 2007, **127**, 194504.

22 C. Norenberg, D. F. Leigh, D. Cattaneo, K. Porfyrakis, A. L. Bassi, C. S. Casari, M. Passoni, J. H. G. Owen and G. A. D. Briggs, *J. Phys.: Conf. Ser.*, 2008, **100**, 052080.

23 D. F. Leigh, C. Norenberg, D. Cattaneo, J. H. G. Owen, K. Porfyrakis, A. Li Bassi, A. Ardavan and G. A. D. Briggs, *Surf. Sci.*, 2007, **601**, 2750–2755.

24 Y. Shirai, L. Cheng, B. Chen and J. M. Tour, *J. Am. Chem. Soc.*, 2006, **128**, 13479–13489.

25 T. M. Willey, A. L. Vance, C. Bostedt, T. van Buuren, R. W. Meulenberg, L. J. Terminello and C. S. Fadley, *Langmuir*, 2004, **20**, 4939–4944.